

Article

Efficient Trajectory Planning for Optimizing Energy Consumption and Completion Time in UAV-Assisted IoT Networks

Mengtang Li ^{1,*}, Guoku Jia ^{1,†}, Xun Li ² and Hao Qiu ²

¹ School of Intelligent Systems Engineering, Shenzhen Campus, Sun Yat-Sen University, Shenzhen 518107, China; jiagk@mail2.sysu.edu.cn

² Department of Electrical and Computer Engineering, Vanderbilt University, Nashville, TN 37240, USA; xun.li@vanderbilt.edu (X.L.); hao.qiu@vanderbilt.edu (H.Q.)

* Correspondence: limt29@mail.sysu.edu.cn

† These authors contributed equally to this work.

Abstract: Quadrotor unmanned aerial vehicles (UAVs) have emerged as ubiquitous and agile robots and data carriers within the framework of the future Internet of Things (IoT) and mobile wireless networks. Yet, the insufficient onboard battery necessitates the optimization of energy consumption for both the UAV and IoT devices while ensuring that communication requirements are met. This paper therefore proposes a more accurate and mathematically tractable model for characterizing a UAV's energy consumption concerning desired trajectories. This nonlinear model takes into account the UAV's dynamics, brushless direct current (BLDC) motor dynamics, and aerodynamics. To optimize the communication time between IoT devices and the UAV, IoT devices are clustered using a modified GAK-means algorithm, with dynamically optimized communication coverage radii. Subsequently, a fly-circle-communicate (FCC) trajectory design algorithm is introduced and derived to conserve energy and save mission time. Under the FCC approach, the UAV sequentially visits the cluster centers and performs circular flight and communication. Transitions between cluster centers are smoothed via 3D Dubins curves, which provide physically achievable trajectories. Comprehensive numerical studies indicate that the proposed trajectory planning method reduces overall communication time and preserves UAV battery energy compared to other benchmark schemes.

Keywords: nonlinear systems; mathematical modeling; trajectory planning; UAV

MSC: 70E60



Citation: Li, M.; Jia, G.; Li, X.; Qiu, H. Efficient Trajectory Planning for Optimizing Energy Consumption and Completion Time in UAV-Assisted IoT Networks.

Mathematics **2023**, *11*, 4399.

<https://doi.org/10.3390/math11204399>

math11204399

Academic Editor: Konstantin Kozlov

Received: 13 September 2023

Revised: 7 October 2023

Accepted: 20 October 2023

Published: 23 October 2023



Copyright: © 2023 by the authors. Licensee MDPI, Basel, Switzerland. This article is an open access article distributed under the terms and conditions of the Creative Commons Attribution (CC BY) license (<https://creativecommons.org/licenses/by/4.0/>).

1. Introduction

Due to low cost, high mobility, and vertical take-off and landing advantages [1,2], unmanned aerial vehicles have found widespread application in mobile communication networks [3], such as UAV-aided ubiquitous coverage [4], UAV-aided relaying [5], and UAV-aided information dissemination and data collection [6]. Generally, UAVs are deployed to fly within certain wireless sensor networks (WSNs), which consist of numerous IoT devices distributed throughout space to collect or transmit data [7,8]. Several protocols have been developed for generating UAV flight trajectories to facilitate mobile data collection tasks [9]. With the extensive research and development in UAV technology, various effective controllers have been designed to ensure precise UAV trajectory tracking. These controllers include simple PID control, LQ control, backstepping control, and sliding mode control [10–12]. Recent advancements in controller design have further enhanced UAV flight agility and trajectory tracking capabilities. Lee et al. introduced the renowned geometric tracking control method, enabling highly accurate tracking even for aggressive trajectories [13,14]. Quan et al. developed a practical distributed controller that enables UAVs to accurately navigate through virtual tubes, enhancing trajectory tracking

performance [15]. Additionally, Zhu et al. designed a nonlinear integral sliding mode attitude controller using the triple-step method to enable UAVs to withstand unknown disturbances [16].

Nevertheless, despite the significant breakthroughs achieved in UAV controllers, effective trajectory planning for UAV-assisted networks remains an area of active exploration and growing interest [17]. Specifically, due to the limited onboard battery capacity of UAVs, there is a pressing need for trajectory optimization concerning both energy consumption and completion time [3]. Furthermore, when ground nodes are disposable with limited power supplies, the optimization of the UAV's trajectory must take into account the energy consumption of these ground nodes [18]. In light of these challenges, extending the lifespan of UAV-aided wireless communication networks becomes imperative. Consequently, the optimization of energy-efficient and time-effective trajectory planning for UAVs has emerged as a critical component of network management [3,17]. The following subsections provide a comprehensive review of related works, with a primary focus on energy consumption models and optimal trajectory design.

1.1. Energy Consumption Model

Before designing energy-optimized trajectories for UAVs within mobile networks, it is essential to develop an accurate energy consumption model for quadrotor UAVs. Current UAV energy consumption models can be classified into three types.

The first is data fitting with empirical power data obtained under various flight conditions using an onboard power sensor [19]. Subsequently, an energy consumption curve is fitted against user-defined variables, such as flight speed [20]. Note that the resulting energy consumption model is highly contingent upon experimental conditions and physical attributes, rendering it non-universal across all UAV models. The second type is based on classical helicopter theory [21,22]. Zeng et al. derived an energy consumption model for rotary-wing UAVs based on this theory. It comprehensively considered the profile power, induced power, and parasite power [23]. However, it is worth noting that helicopters and quadrotor UAVs differ in their physical structures, which may lead to inaccurate energy consumption results. The third type considers the unique structure of a quadrotor UAV. Caitlin et al. established the dynamic equations of quadrotor UAVs using the Newton–Euler equation, taking into account the influence of relative wind speed, ground effects, and interferences from nearby UAVs [24]. Bouabdalla et al. deduced the thrust, hub force, and torque coefficients of small quadrotor UAVs based on the blade element theory. This model considers the differences in blade structure between quadrotors and helicopters, resulting in a more comprehensive and accurate deduction of the influence of aerodynamics [25]. Hoffmann et al. studied the influence of three aerodynamic effects, namely, vortex ring state, blade flapping, and the interference caused by the fuselage, resulting in a complex thrust analysis [26]. While the above works focused on the impact of aerodynamics on quadrotor UAVs, they did not derive the energy consumption from the perspective of quadrotor UAVs' fundamental actuators, namely, BLDC motors.

To address these gaps, a novel energy consumption model considering quadrotor dynamics, aerodynamics, and BLDC motor dynamics has previously been developed by the authors [27], which is more suitable for energy-efficient trajectory planning for UAV-assisted networks.

1.2. Trajectory Optimization Method

Subsequently, an optimal trajectory can be intricately designed to conserve UAV energy through the application of suitable energy consumption models. In the context of the mobile communication network, classification can be made based on the number of UAVs and IoT users, resulting in three distinct configurations: the one-to-one scenario [28], the one-to-multi scenario [29], and the multi-to-multi scenario [30]. The one-to-one scenario aims to minimize the flight distance required to complete the communication task, effectively transforming it into a traveling salesman problem [31]. The one-to-multi scenario, which

involves more optimization constraints compared to the one-to-one scenario, has garnered greater interest and can be readily extended to the multi-to-multi scenario.

Considering the multi-channel communication capabilities of a UAV within a wireless network, IoT devices can be clustered based on their locations, a problem akin to the disk cover problem [32]. K-means is a widely adopted and practical algorithm for clustering multiple objects. Galkin et al. employed the K-means algorithm to partition airborne access points into K clusters and subsequently deployed the UAV at the center of each cluster, thereby alleviating the load on macrocells and achieving superior signal strength compared to static picocell alternatives [33]. Li et al. introduced the BTK-means algorithm, which addresses the issue of millimeter-wave signal blockage and facilitates the clustering of ground users and UAV deployment [34]. Qu et al. proposed the UBK-means algorithm, which considers user bandwidth requirements to determine the number of centers, resolving bandwidth limitations in emergency scenarios [35]. However, one limitation of the classical K-means algorithm is its sensitivity to the initial random selection of cluster centers. Consequently, intelligent clustering of IoT devices is imperative to enhance the performance of both the UAV and the IoT network, with a focus on energy efficiency.

Mozaffari et al. employed the circle packing algorithm to determine the minimum number of disks [36,37]. However, this method's primary focus on achieving complete coverage of circular areas results in significant cross-coverage issues, as it does not consider the location information of IoT devices. Lyu et al. proposed an algorithm for placing UAV base stations along a spiral line, utilizing the maximum coverage radius of a UAV to cover IoT devices, with the objective of minimizing the number of disks [32]. Zeng et al. applied this spiral algorithm to cluster IoT devices, and the traveling salesman problem (TSP) algorithm was integrated to minimize completion time [30]. Nevertheless, the coverage radius of the disk was chosen as the maximum value of the UAV's communication range. In cases where some IoT devices are highly aggregated and distant from others, this additional coverage radius results in energy wastage.

To address this aforementioned gap, this paper introduces a variable-radius disk cover method based on the GAK-means algorithm, which dynamically clusters IoT devices based on their locations. This approach enables the design of better-optimized trajectories to achieve efficient energy consumption for both the UAV and IoT devices.

1.3. Overview of the Proposed Method

In this study, a wireless communication network is investigated where one single quadrotor UAV is deployed as a mobile base station to establish communication with multiple IoT devices. The objective is to optimize the energy consumption of both the UAV and IoT devices while ensuring the communication requirements of each IoT device are met. Firstly, the energy consumption model of a quadrotor UAV is formulated. Secondly, a trajectory planning algorithm is designed to optimize the energy consumption of the UAV and IoT devices. The well-established communication model proposed by Al-Hourani et al. [38] is employed to determine the maximum radius of communication coverage. IoT devices located beyond this maximum radius are deemed invalid connections. Within the communication coverage, IoT devices are clustered based on Euclidean distance to minimize total communication time with the UAV. Upon resolution of the disk cover problem, the centers of clusters are connected to minimize distance. An efficient, high-quality approximate solution is obtained by applying a well-established TSP-solving algorithm. Finally, to further enhance the energy efficiency of the UAV, a novel FCC trajectory design is proposed, which combines circular trajectories and 3D Dubins trajectories.

The remainder of this paper is organized as follows: In Section 2.1, the derivation of the energy consumption model of a quadrotor UAV concerning a desired trajectory is introduced. Section 2.2 covers the presentation of the communication model of the wireless network. In Section 2.3, an energy-optimized trajectory design algorithm is proposed, which is based on the modified GAK-means algorithm, TSP algorithm, and Dubins curve, within a UAV-assisted mobile communication network. Section 3 presents numerical

studies to evaluate the proposed methodology. The final section comprises the summary and conclusion.

2. Materials and Methods

2.1. UAV Energy Consumption Model

The fundamental idea of this energy consumption model is to calculate the electric power provided by the four BLDC motors of a quadrotor UAV concerning an input trajectory. The energy model takes into account detailed nonlinear dynamics, including quadrotor dynamics, aerodynamics, and BLDC motor dynamics, which are briefly introduced here to explain the calculation of energy consumption. A more comprehensive derivation can be found in a previous work [27].

2.1.1. Dynamic Model of a Quadrotor UAV

Figure 1 illustrates the free body diagram of a general quadrotor UAV. A rigid body frame $\{b_1, b_2, b_3\}$ and an inertial reference frame $\{e_1, e_2, e_3\}$ are established. The dynamic equation for a UAV is as follows:

$$\begin{bmatrix} T \\ M_1 \\ M_2 \\ M_3 \end{bmatrix} = \begin{bmatrix} k_f & k_f & k_f & k_f \\ 0 & -lk_f & 0 & lk_f \\ -lk_f & 0 & lk_f & 0 \\ -k_\tau & k_\tau & -k_\tau & k_\tau \end{bmatrix} \begin{bmatrix} \omega_1^2 \\ \omega_2^2 \\ \omega_3^2 \\ \omega_4^2 \end{bmatrix} \tag{1}$$

where T is the net thrust, M is the resultant moment, k_τ and k_f are the torque and the thrust coefficients, respectively, and $\omega_i, i = 1, \dots, 4$ are the angular velocity of the rotors. To simplify the formula, we convert scalars into vector representations, with $\|F\| = T, F \in \mathbb{R}^3$ and $M = [M_1, M_2, M_3]^T$. Given a desired trajectory $q_d(t)$ in frame $\{e\}$, the thrust F_d and moment M_d can be obtained by:

$$F_d = m\ddot{q}_d + mge_3 + \frac{1}{2}\rho S_F \|\dot{q}_d\| \dot{q}_d \tag{2}$$

$$M_d = J\dot{\Omega}_d + \Omega_d \times J\Omega_d \tag{3}$$

$$\Omega_d = (R_d^T \dot{R}_d)^\vee \tag{4}$$

$$\dot{\Omega}_d = (\dot{R}_d^T \dot{R}_d + R_d^T \ddot{R}_d)^\vee \tag{5}$$

For the sake of space, the exact expressions of $R_d, \dot{R}_d,$ and \ddot{R}_d can be found in [27,39] and the explanation of all other parameters are in Table 1. Note that $R_d, \dot{R}_d, \ddot{R}_d, F_d,$ and M_d are all determined by the desired trajectory $q_d(t)$. A fundamental requirement is the trajectory must be third-order differentiable to accommodate \ddot{q}_d .

2.1.2. Thrust Coefficient and Torque Coefficient

The thrust coefficient k_f and torque coefficient k_τ are calculated by $k_f = t_c \rho s A r^2$ and $k_\tau = q_c \rho s A r^3$ [21]. The thrust and torque coefficient parameters $t_{c,i}$ and $q_{c,i}$ can be obtained as [21]:

$$t_{c,i} = \frac{a}{4} \left[\frac{2}{3} \theta_0 \left(1 + \frac{3V^2}{\omega_i^2 r^2} \right) - \lambda_i \right], t_c = \frac{1}{4} \sum_{i=1}^4 t_{c,i} \tag{6}$$

$$q_{c,i} = \frac{\delta}{8} \left(1 + \frac{3V^2}{\omega_i^2 r^2} \right) + (1+k) \lambda_i t_c + \frac{1}{8} d_0 \frac{V^2}{\omega_i^2 r^2}, q_c = \frac{1}{4} \sum_{i=1}^4 q_{c,i} \tag{7}$$

$$\lambda_i = \frac{\left(\sqrt{\left(\frac{mg}{8\rho\pi r^2}\right)^2 + \frac{V^4}{4} - \frac{V^2}{2}}\right)^{\frac{1}{2}}}{\omega_i r} \tag{8}$$

The description of the parameters are presented in Table 1. Note that $t_{c,i}$ and $q_{c,i}$ are both affected by the forward speed V and rotor speed ω_i .

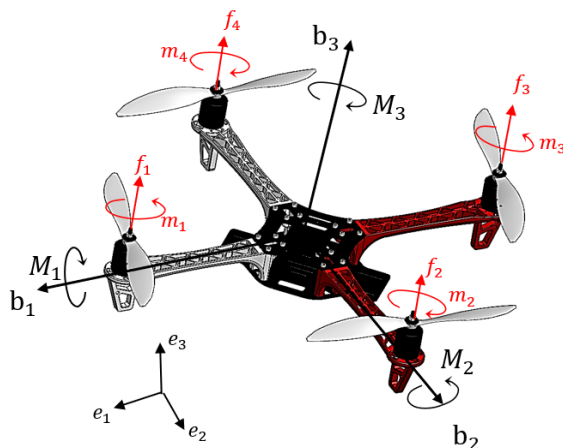


Figure 1. Free body diagram of a general quadrotor UAV. $\{e\}$ represents the inertial reference frame, $\{b\}$ stands for the rigid body frame, f_i and M_i are thrusts and torques produced by the four rotor blades.

Table 1. Physical parameters of a UAV [26,40].

Parameter	Value	Parameter	Value
mass	$m = 1.3 \text{ kg}$	gravity	$g = 9.8 \text{ N/kg}$
rotor radius	$r = 0.12 \text{ m}$	rotor location	$l = 0.4 \text{ m}$
lift slope	$a = 5.7$	rotor disk area	$A = 0.0452 \text{ m}^2$
fuselage equivalent flat plate area	$S_F = 0.003 \text{ m}^2$	air density	$\rho = 1.225 \text{ kg/m}^3$
collective pitch angle	$\theta_0 = 0.13 \text{ rad}$	profile drag coefficient	$\delta = 0.012$
incremental correction factor	$k = 0.1$	rotor solid	$s = 0.05$
viscous damping coefficient	$D_f = 2 \times 10^{-4} \text{ Nms/rad}$	voltage constant	$K_E = 0.01 \text{ Vs/rad}$
motor resistance	$R = 0.2 \Omega$	moment of inertia x	$J_x = 0.082 \text{ kgm}^2$
moment of inertia y	$J_y = 0.084 \text{ kgm}^2$	moment of inertia z	$J_z = 0.137 \text{ kgm}^2$

2.1.3. BLDC Motor Dynamic Model

With the current and voltage across the i -th BLDC motor measured, the power required for a single BLDC motor of the UAV is therefore [41]:

$$\mathbb{P}_i(t) = \frac{R}{K_T^2} [D_f \omega_i + m_L(\omega_i)]^2 + \frac{K_E \omega_i}{K_T} [D_f \omega_i + m_L(\omega_i)] \tag{9}$$

The description of above parameters are in Table 1. Therefore, for a given fly time T_{fly} along a given trajectory $q_d(t)$, the UAV consumes the following amount of energy:

$$\mathbb{E}(T_{fly}) = \int_0^{T_{fly}} \sum_{i=1}^4 \mathbb{P}_i(t) dt \tag{10}$$

Note that the only variable of the above equation is $\omega_i, i = 1, \dots, 4$.

2.1.4. Energy Consumption Calculation

With all the dynamic models developed previously, (1) can be rewritten as functions of the desired trajectory $q_d(t)$ via substituting (2), (3), (6), and (7) into (1):

$$\sum_{i=1}^4 (C_1 \omega_i^2 + C_2 \omega_i + C_3) = T_d(q_d) \tag{11a}$$

$$IC_1(\omega_4^2 - \omega_2^2) + IC_2(\omega_4 - \omega_2) = M_{1d}(q_d) \tag{11b}$$

$$IC_1(\omega_3^2 - \omega_1^2) + IC_2(\omega_3 - \omega_1) = M_{2d}(q_d) \tag{11c}$$

$$\sum_{i=1}^4 (-1)^i (D_1 \omega_i^2 + D_2 \omega_i + D_3 \frac{1}{\omega_i}) = M_{3d}(q_d) \tag{11d}$$

where $C_1 = \frac{1}{6} \rho s A a \theta_0 r^2$, $C_2 = -\frac{1}{4} \rho s A a v_{i0} r$, $C_3 = \frac{1}{2} \rho s A a \theta_0 V^2$, $D_1 = \frac{1}{8} \delta \rho s A a r^3$, $D_2 = \frac{1}{6} (1 + k) v_{i0} \rho s A \theta_0 r^2$, $D_3 = \frac{1}{2} (1 + k) v_{i0} \rho s A a \theta_0 V^2 + \frac{1}{8} \rho S_F V^3$. $C_1, C_2, C_3, D_1, D_2, D_3$ are coefficients which are determined by an input trajectory $q_d(t)$. Thus, the rotor speed ω_i can be obtained by (11) and is then substituted into (9) and (10) to solve for BLDC motor power $\mathbb{P}(t)$ and energy $\mathbb{E}(T_{fly})$ of a UAV.

The blue line depicted in Figure 2 illustrates the relationship between the forward speed, V , and the propulsion power of a quadrotor UAV, \mathbb{P} , which is based on the condition of a linear trajectory with a constant speed represented by $q_d(t) = [Vt; const; const]^T$. As the forward speed of the quadrotor UAV increases, the propulsion power initially decreases before rising again, similar to the power curve of helicopters [26]. This phenomenon results from the effect of forward speed on the torque and thrust coefficients. Consequently, the power consumption of the quadrotor UAV when moving forward at low speed is lower than during hovering. Moreover, there exists a specific speed, denoted as V_{minE} , which maximizes the total travel distance for a fixed amount of energy. The graphical determination of V_{minE} involves drawing a tangential line from the origin to the power curve [23]. It is worth noting that the UAV speed that minimizes propulsion power, referred to as V_{minp} , is not the optimal speed for achieving the minimum energy consumption. This is because it requires more time to cover a fixed distance compared to V_{minE} .

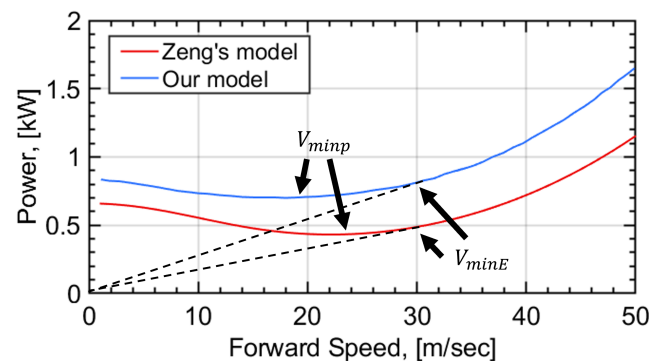


Figure 2. The relationship between forward speed V and UAV’s entire propulsion power \mathbb{P} (the blue and red lines are simulated from the proposed model and the model by Zeng et al. [23], respectively). V_{minE} maximizes the total travel distance, while V_{minp} minimizes propulsion power.

The red line in Figure 2 is calculated using the model proposed by Zeng et al. [23]. It should be noted that since this model is based on the helicopter theory, meaning only one rotor is considered during the energy calculation, the resulting power is manually multiplied by four times to account for the quadrotor UAV configuration. The patterns between the forward speed V and the total propulsion power \mathbb{P} from Zeng’s model and the proposed model are analogous. However, the proposed model fundamentally enhances the accuracy of energy consumption calculation for a quadrotor UAV in three key aspects: First, while a helicopter maintains a relatively constant rotor blade speed and achieves

attitude and velocity adjustments through intricate mechanical alterations of propeller geometric inclination, a quadrotor UAV relies on fixed rotor blade pitch angles and adjusts the angular velocity of its four rotor blades for attitude and velocity control. Second, whereas a helicopter employs large main blades for primary thrust and small tail wings to counteract reaction torque due to air resistance on main blade rotation, a quadrotor UAV utilizes four equally positioned propellers to provide motion force and torque. Lastly, unlike a helicopter, the dynamic coupling of the four blades in a quadrotor UAV renders the simultaneous specification of forward speed and alteration of rotor blade rotation speed impractical.

2.2. Communication Model for Mobile IoT Networks

The communication model is developed in this section, followed by characterization of the relationship between the communication coverage radius and the altitude of the UAV. The model considers a rectangular area, where a number of IoT devices are deployed, and a UAV is dispatched to communicate with a set of N IoT devices simultaneously, as depicted in Figure 3. The objective is to concomitantly optimize the energy consumption of the UAV and IoT devices by means of UAV trajectory planning.

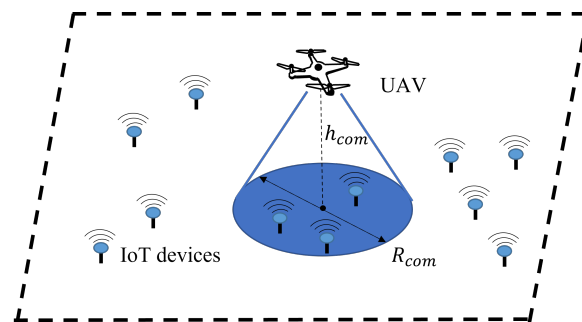


Figure 3. A UAV gathering data from a set of N IoT devices simultaneously in a wireless communication network.

The UAV’s 3D coordinate is denoted as $\mathbf{q}(t) = [x_{uav}(t), y_{uav}(t), z_{uav}(t)]^T$, and the coordinate of i -th IoT device is $\mathbf{u}_i = [x_{IoTi}, y_{IoTi}, 0]^T$. Hence, the time-dependent distance between i -th IoT device and the UAV is:

$$d_i(t) = \|\mathbf{q}(t) - \mathbf{u}_i\| \tag{12}$$

This paper adopts the communication channel model proposed by Al-Hourani et al. [38] to obtain the UAV’s optimum altitude that maximizes ground coverage. Specifically, the UAV can receive two types of signals including line-of-sight (LoS) and non-line-of-sight (NLoS) signals. The probability of occurrence for each group is determined by various factors, with their corresponding probabilities expressed as follows:

$$P(LoS) = \frac{1}{1 + \zeta_1 e^{-\zeta_2(\theta_s - \zeta_1)}} \tag{13}$$

$$P(NLoS) = 1 - P(LoS) \tag{14}$$

where ζ_1 and ζ_2 are S-curve parameters depending on the environment conditions and θ is the elevation angle, $\theta_s = \frac{180}{\pi} \arctan(h_{com} / R_{com})$, R_{com} is radius of communication coverage, and h_{com} is UAV height. The pathlosses of the LoS group and NLoS group are:

$$PL_{LoS} = 20 \log \frac{4\pi F_c d_i(t)}{c} + \eta_{LoS} \tag{15}$$

$$PL_{NLoS} = 20\log\frac{4\pi F_c d_i(t)}{c} + \eta_{NLoS} \tag{16}$$

where F_c is the transmission frequency, c is the light speed. The first terms of (15) and (16) represent the free space pathloss between the UAV and an IoT device. The second terms represent the mean value of the excess path loss. The total mean path loss between the UAV and an IoT device, following the expectation rule, can be obtained as follows:

$$PL_{mean} = PL_{LoS} \cdot P(LoS) + PL_{NLoS} \cdot P(NLoS) \tag{17}$$

Given a maximum allowable pathloss PL_{max} and environment condition, (17) becomes:

$$PL_{max} = \frac{\eta_{LoS} - \eta_{NLoS}}{1 + \zeta_1 e^{-\zeta_2[\arctan(\frac{h}{R}) - \zeta_1]}} + 10\log(h_{com}^2 + R_{com}^2) + 20\log\frac{4\pi F_c}{c} + \eta_{NLoS} \tag{18}$$

Although the explicit expression of R_{com} or h_{com} cannot be obtained directly, it can be acquired numerically. Assuming $F_c = 2 \times 10^9$ Hz, $c = 3 \times 10^8$ m/s, $PL_{max} = 10$ dB, Figure 4 depicts the relationship between R_{com} and h_{com} with the environment parameters [42] shown in Table 2.

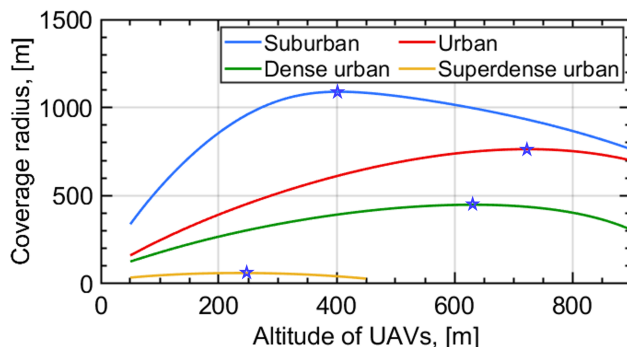


Figure 4. Coverage radius versus altitude for different environment. Stars mark the maximum coverage radii.

Table 2. Communication and environment parameters [42].

Environment	Parameters ($\zeta_1, \zeta_2, \eta_{LoS}, \eta_{NLoS}$)
Suburban	(4.88, 0.43, 0.10, 21.00)
Urban	(9.61, 0.16, 1.00, 20.00)
Dense urban	(12.08, 0.11, 1.60, 23.00)
Superdense urban	(27.23, 0.08, 2.30, 34.00)

Hence, the altitude of the UAV can be established in accordance with the corresponding coverage radius. It is noteworthy that only one maximum coverage radius exists. If the distance between the UAV and an IoT device surpasses this threshold, the connection is deemed unsuccessful. Additionally, a UAV typically operates within certain altitude constraints, often remaining below 300 m. During interactions with IoT devices, the received signal-to-noise ratio for i -th IoT device is expressed as:

$$\gamma_i(t) = \frac{\mathbb{P}_{tran}}{d_i(t)^2 \sigma^2 PL_{mean}} \tag{19}$$

where \mathbb{P}_{tran} represents the transmit power of the UAV, and σ^2 is the white noise power. The channel capacity based on the path loss model is then derived as follows:

$$C_i^{rate}(t) = B \log_2(1 + \gamma_i(t)) \quad (20)$$

where B denotes the channel bandwidth. The cumulative amount of data within a communication period T is:

$$Q_i^{data} = \int_0^T C_i^{rate}(t) dt \quad (21)$$

Note that the communication time between the UAV and an IoT device is affected by several key parameters. Among them, the communication bandwidth, transmission power, and white noise power are all fixed values under specified conditions. Thus, the communication time only depends on the distance between the UAV and the device. In addition, when the UAV communicates with multiple devices at the same time, the communication time will depend on the device with the farthest distance within the communication range.

2.3. Trajectory Planning

2.3.1. Optimization Problem

To accomplish the task described in Figure 3, where a group of K IoT devices are to be communicated by a quadrotor UAV [32], a carefully planned trajectory $q(t)$ should be designed for a UAV, considering the completion time and energy consumption of the UAV and the IoT devices. The optimization problem can be stated as:

$$\min_{q(t)} = \mathbb{E}_{UAV}(q(t)) \quad (22)$$

$$\int_0^{T_k} C_k^{rate}(t) dt \geq Q_k^{data} \quad (23)$$

$$\mathbb{E}_{UAV} \leq \mathbb{E}_{max} \quad (24)$$

$$\|\dot{q}(t)\| \leq V_{max} \quad (25)$$

$$\|\ddot{q}(t)\| \leq a_{max} \quad (26)$$

where (23) represents the requirement for information gathering, signifying that data from all IoT devices within the k -th cluster must be collected entirely. Equation (24) sets the limitation on UAV energy consumption, with \mathbb{E}_{max} representing the maximum energy that the UAV's battery can provide. Equations (25) and (26) stipulate that the UAV's speed and acceleration cannot exceed their respective maximum limits. Straightforwardly, the optimal energy consumption solution and the optimal completion time solution are inherently contradictory and therefore cannot be simultaneously attained. Consequently, in addressing the optimization problem above, precedence is given to energy optimization. The optimization of completion time is subsequently achieved through the refinement of both the flight and communication processes, as elaborated in the following subsections.

2.3.2. Disk Cover Clustering

To optimize the energy consumption of the UAV, the IoT devices are clustered into disk-shaped regions of various sizes, ensuring that they remain within the maximum communication coverage. Simultaneously, to optimize the energy consumption of the IoT devices, as well as the devices' operating time, the total distance between the UAV and IoT devices within the same cluster region should be minimized. The K-means algorithm is a widely used unsupervised clustering technique that involves partitioning a given dataset

into K clusters, where K is a predefined number of clusters. The algorithm operates through a series of iterative steps, where each data point is assigned to its nearest cluster center, and the centers of the clusters are recalculated based on the newly assigned points. The objective function aims at minimizing the sum of distances from all IoT devices to their respective cluster centers:

$$J_{obj} = \sum_{j=1}^K \sum_{u_i \in \Theta_j} \|u_i - \bar{u}_{\in \Theta_j}\|^2 \tag{27}$$

where Θ_j is j -th cluster, u_i is the location of IoT devices in cluster Θ_j , and $\bar{u}_{\in \Theta_j}$ is the mean value of all IoT devices' coordinate in cluster Θ_j . However, one limitation of the classical algorithm is that it is prone to sensitivity towards cluster centers' initial positions, resulting in different final clustering solutions. Therefore, the modified GA is embedded with the classical K-means algorithm to avoid local convergence.

In this work, coordinates of all the cluster centers are concatenated as chromosomes for the GA algorithm. For example, if the coordinates of the four cluster centers are (220, 150), (1230, 15), (140, 112), (251, 3), the chromosome code is (220, 150, 1230, 15, 140, 112, 251, 3). Subsequently, the constituent parameters of these chromosomes are aggregated and subjected to mutation operations to generate novel solutions within the ensuing generation. These novel solutions are rigorously assessed based on their efficacy in addressing the specific problem at hand. This evaluative process is realized through the employment of a fitness function, wherein chromosomes endowed with higher values are considered more adept at addressing the problem. The fitness function is architected as follows:

$$fit = \frac{1}{1 + J_{obj}} \tag{28}$$

The selection operation $f_{selec}()$ used here is the championship selection method, namely, selecting two parents randomly and returning the one with the highest fitness. The cross operation used here is the single point crossing method. A single crossover point is arbitrarily chosen in the individual code string, and the chromosome is divided into two parts. Both sides of the offspring chromosome are inherited from the corresponding sides of the parent chromosome. Given chromosomes $x_1, x_2 \in \mathbb{R}^{2k}$, the index of the intersection j is between 1 and $2k - 1$. Thus, the new chromosomes after cross operation $f_{cross}()$ are:

$$\begin{aligned} x^1 &= [x^1_{(1:j)}, x^2_{(j+1:2k)}] \\ x^2 &= [x^2_{(1:j)}, x^1_{(j+1:2k)}] \end{aligned} \tag{29}$$

The mutation operation used here is the uniform mutation method. This involves the replacement of the gene value at each location in the individual's coding sequence with a low probability, using random numbers that are uniformly distributed within a specific range. Given a chromosome $x^3 \in \mathbb{R}^{2k}$ and a uniformly distributed random vector $x' \in \mathbb{R}^{2k}$, the new chromosome after mutation operation $f_{mute}()$ is:

$$x^3 = x^3 + x' \tag{30}$$

One significant challenge in implementing the GAK-means algorithm is the necessity of predefining the number of cluster centers. It is noteworthy that the maximum radius of the clustered disk decreases as the number of centers increases. When the maximum radius among all disks after clustering falls below the radius limit, the algorithm iteratively adjusts the number of cluster centers. The algorithm is detailed in Algorithm 1, where genetic operations and K-means operations are incorporated into the population evolution process for clustering. This algorithm harnesses the global optimization capabilities of genetic algorithms and the local optimization abilities of the K-means operation. Figure 5 demonstrates a clustering progress. With each disk region, the UAV can efficiently commu-

nicate with multiple devices at the center of each disk, ensuring effective link maintenance. Simultaneously, it minimizes the total distance between the UAV and the IoT devices within a disk, thereby optimizing the total transmission time.

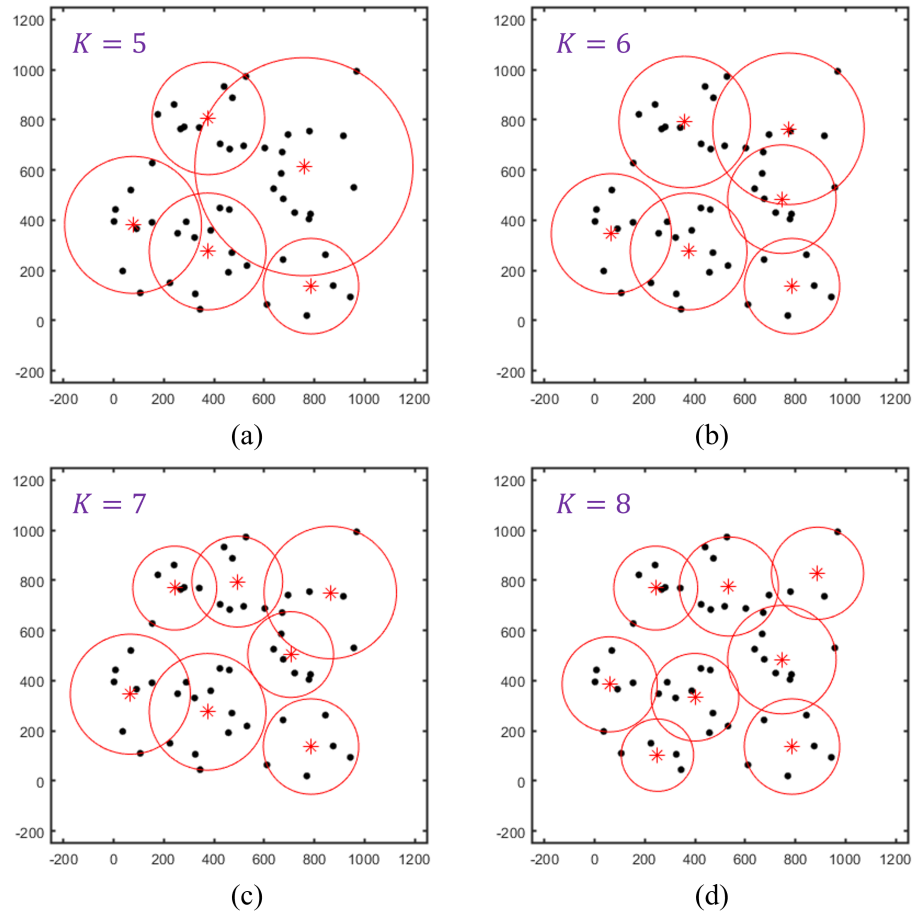


Figure 5. A clustering progress. The IoT devices’ locations in the four figures are the same. The maximum radius of all the disk-shaped clusters after clustering decreases as the number increases. (a) $K = 5$. (b) $K = 6$. (c) $K = 7$. (d) $K = 8$.

Algorithm 1: Disk Cover Problem based on GAK-means Algorithm.

- 1: **Input:** limited coverage radius R_{lim} , population size, mutation probability, crossover probability, maximum iteration number N_{max} , center number $K = 1$, maximum coverage radius $R_{max} = +\infty$
 - 2: **while** $R_{max} > R_{lim}$
 - 3: $K = K + 1$.
 - 4: **for** $i = 1 : N_{max}$.
 - 5: Generate the initial populations and calculate the fitness of chromosomes.
 - 6: $f_{selec}()$, $f_{cross}()$, $f_{mute}()$ and K-means operations. Screen out new populations.
 - 7: **end for**
 - 8: Calculate R_{max} of the chromosome that has the highest $fit()$.
 - 9: **end while**
 - 10: **Output:** K , and the chromosome that has the highest $fit()$.
-

2.3.3. Clustered Disk Connection

Upon completing the disk clustering process, the shortest visiting sequence is established by connecting the centers of clustered disks, thus solving a traveling salesman

problem. Researchers have proposed various solutions for TSP, including genetic algorithms, simulated annealing, and tabu search [43–45]. After determining the optimal visiting sequence, the UAV initially flies in a straight line to a position near the center of the disk region at the optimal speed V_{minE} . Subsequently, it follows a circular trajectory while collecting data from IoT devices. The radius of the circular trajectory is chosen to be R_{cir} , and the velocity is set as V_{cir} . This fly–circle–communicate approach has demonstrated lower energy consumption than hovering flight when optimal speed and circular radius are selected [27].

Note that the communication time for flying around each disk region by the UAV is determined by the data volume of IoT devices within that disk region. The entry and exit positions of the UAV at each disk region must be calculated, and then these positions are connected following the same order as the TSP solution. Additionally, the different radii of the disks are achieved by adjusting the height of the UAV. Consequently, the entry and exit positions that need to be connected exist in a 3D space. To ensure a seamless transition without significant acceleration or deceleration, 3D Dubins curves [46] are employed in this work. These curves are designed to find the shortest smooth path between two points with predetermined orientation angles and bounded curvature. Further details are provided in the following subsection.

2.3.4. Three-Dimensional Dubins Curve Connection

Assuming that circular trajectories are executed by the UAV in a counterclockwise direction, the optimal radius of the circular trajectory, as described previously, has been determined, and the UAV’s altitude has been adjusted accordingly based on the disk radius. The centers of two adjacent circular trajectories are denoted as $O_1(x, y, z)$ and $O_2(x, y, z)$. To obtain the position and directional angle α_{pt2} at the point of entry pt_2 , the projection of circular trajectory O_2 onto the plane containing circular trajectory O_1 , denoted as O'_2 , is shown in Figure 6a. The horizontal distance between the two centers is:

$$S_{D2D} = ||O_1O'_2|| \tag{31}$$

The distance between the center of O_1 and the point pt'_2 is:

$$L_{tan} = \sqrt{S_{D2D}^2 - R_{cir}^2} \tag{32}$$

The orientation angle of at the entry point, pt_2 is therefore:

$$\alpha_{pt2} = \arctan \frac{O_{2y} - O_{1y}}{O_{2x} - O_{1x}} - \arctan \frac{r_{cir}}{L_{tan}} \tag{33}$$

The coordinate of the entry point pt_2 is:

$$pt_{2x} = L_{tan} \cos \alpha_{pt2} + O_{1x} \tag{34a}$$

$$pt_{2y} = L_{tan} \sin \alpha_{pt2} + O_{1y} \tag{34b}$$

$$pt_{2z} = O_{2z} \tag{34c}$$

Note that the altitude of the UAV is determined by the coverage radius of disk in (18). The exit point pt_1 is determined by the entry point and the circular path followed by the UAV during communication, which will be derived in the following part.

When the UAV flies near the center of a disk region and starts to execute the circular trajectory, the UAV starts to communicate with multiple IoT devices at the same time. Assuming that all communication data amount of IoT devices are the same, the fly time of circular trajectory eventually depends on the very IoT device located on the edge of disk where the distance between the UAV and the IoT device is the largest, leading to the smallest communication rate and the largest communication time. The geometric

relationship of communication distance between the UAV and an IoT device is shown in Figure 6b. The distance in between is:

$$S_{U2I}(\phi) = H^2 + L(\phi)^2 = H^2 + R_{disk}^2 + R_{cir}^2 - 2R_{disk}R_{cir}\cos(\phi) \tag{35}$$

where R_{disk} is the coverage radius of the UAV, and R_{cir} is the radius of the UAV circular trajectory. Therefore the distance $S_{U2I}(\phi)$ is a function of time, as $\phi = V_{cir}/R_{cir} \cdot t$. Thus, the communication rate is a function of communication distance according to (20), and channel capacity C_{rate} is a function of time. Then, the total communication time T_{cir} can be calculated by Equation (21). Therefore, the arc of the circular trajectory left during communication is:

$$\Phi = \frac{V_{cir}}{R_{cir}} T_{cir} \tag{36}$$

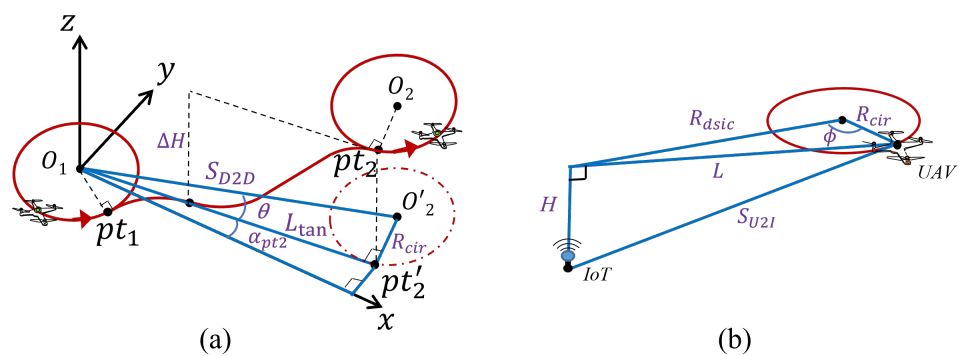


Figure 6. (a) Calculation of the entry and exit points of a Dubins curve. (b) Calculation of the distance between the UAV and an IoT device.

Finally, the proposed FCC trajectory is generated via linking the exit curve of current arc, the transition curve in a vertical plane, and the entry curve of the next circle, as summarized in Algorithm 2.

Algorithm 2: FCC Trajectory Planning Algorithm.

- 1: **Input:** amount of data Q_{data} , IoT device positions $\{u_i\}$, parameters of the UAV in Table 1.
 - 2: Run Algorithm 1 to obtain K and the center of the disk.
 - 3: Run TSP algorithm to obtain the visiting sequence $\{\hat{\pi}_k\}$.
 - 4: Choose V_{cir} and R_{cir} for the circular path, and V_{minE} for transition straight path.
 - 5: **for** $i = 1 : K$
 - 6: Compute entry and exit points pt_1 and pt_2 of disk $m(\hat{\pi}_k)$.
 - 7: Connect entry and exit points by Dubins curve.
 - 8: **end for**
 - 9: **Output:** UAV's trajectory.
-

3. Results

In this section, we present numerical studies to assess the performance of the proposed trajectory design methodology. Two representative examples are provided, with the first showcasing a dense distribution of IoT devices and the second with a sparser distribution. All cases are simulated with dense urban environment parameters $(\zeta_1, \zeta_2, \eta_{LoS}, \eta_{NLoS}) = (12.08, 0.11, 1.60, 23.00)$.

The first illustrative example involves 50 IoT devices, each with a data amount of 0.5 Mb, and their coordinates are randomly distributed between 0 and 1000 m as depicted in Figure 7. Another example comprises 20 IoT devices, each with a data amount of 2 Mb, and their coordinates are randomly distributed between 0 and 1500 m as shown in Figure 8.

The UAV's transmission power is set at 5 W, the bandwidth is 60 MHz, and the white noise power is -110 dBm.

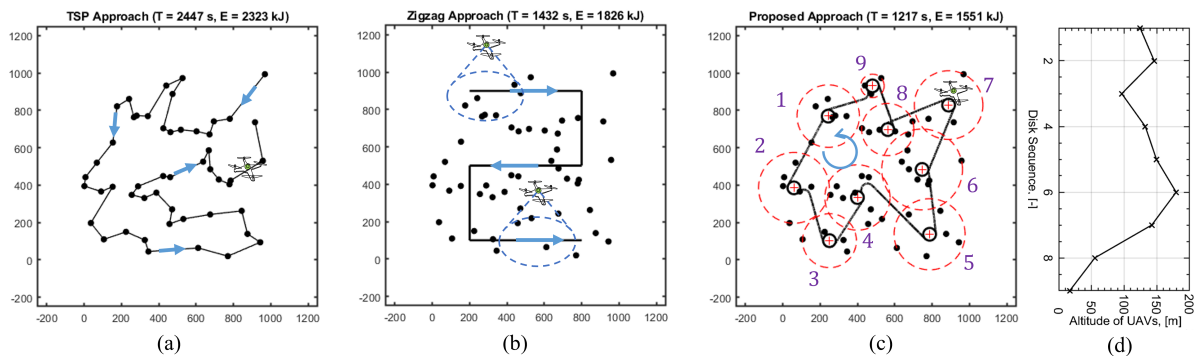


Figure 7. Comparison of example 1 of the UAV trajectories with different approaches. Small black dots represent IoT devices. (a) TSP approach. (b) Zigzag approach. (c) Proposed FCC approach. (d) FCC approach's corresponding height changes.

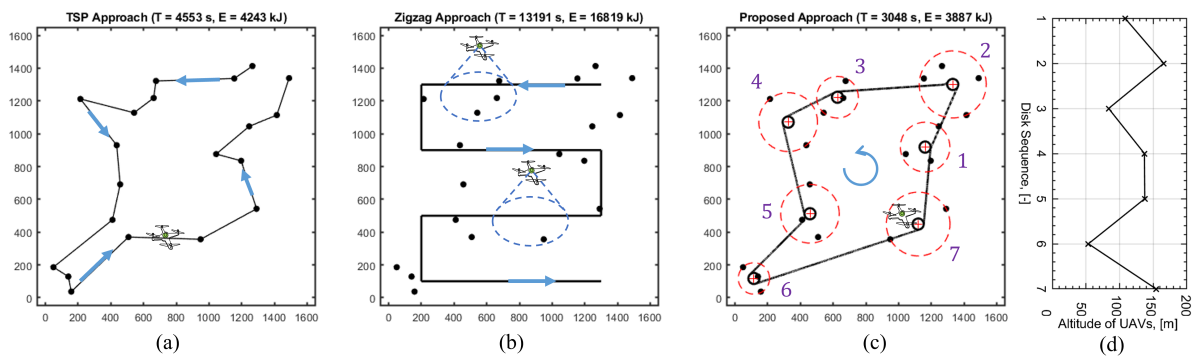


Figure 8. Comparison of example 2 of the UAV trajectories with different approaches. Small black dots represent IoT devices. (a) TSP approach. (b) Zigzag approach. (c) Proposed FCC approach. (d) FCC approach's corresponding height changes.

3.1. Benchmark TSP Approach

First, the direct TSP design is employed as the benchmark, where the UAV flies sequentially to each IoT device and performs hover–communicate with every device. The height of the UAV is set as $H = 100$ m, and the speed during the straight-line segments is set to V_{minE} to minimize energy consumption. Simulation results indicate that 2247 s are required for the task's completion in Figure 7a, with a total energy consumption of 2323 kJ. In the second scenario, the task depicted in Figure 8a necessitates 4553 s for completion by the UAV, with a total energy consumption of 4243 kJ.

3.2. Zigzag Approach

Next, the zigzag approach, also referred to as the strip-based approach, is considered. The zigzag approach is often employed in the context of pesticide-spraying UAV or floor-sweeping robots [47]. In this approach, a rectangular area is efficiently covered by the UAV as it moves back and forth along lines that are either perpendicular or parallel to the boundary. The zigzag approach adopts the 'fly-and-communicate' protocol, wherein IoT devices are communicated with by the UAV while in flight. Assuming an absence of limitations on the number of devices that can simultaneously communicate with the UAV [47], it becomes necessary for the UAV to establish communication with as many devices as possible to achieve energy optimization. Consequently, the maximum coverage radius is employed for scanning purposes. To optimize communication performance, special attention is directed towards ensuring successful reception of shared information

by IoT devices located farthest from the UAV, as they tend to be the limiting factor. As depicted in Figure 9, a hexagon is employed to approximate the circular communication coverage [47]. Taking the i -th IoT device as an illustrative example for the sweep border, if it can successfully receive the information, all IoT devices within the coverage area will be able to meet the requirements.

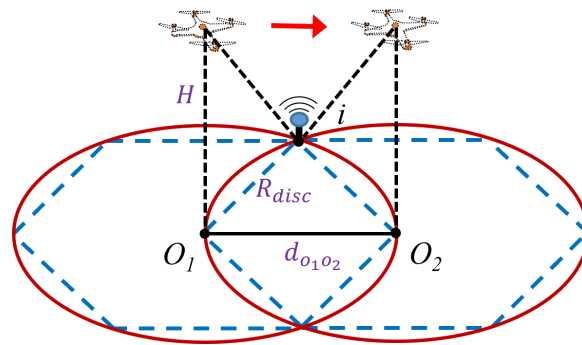


Figure 9. Sweep border for the zigzag approach.

When the UAV's projection on the ground is positioned between the two circle centers, the i -th device is fully covered by the UAV. The distance between the two circle centers is denoted as $d_{O_1O_2}$, which has been determined to be equal to R_{disk} through geometric derivation. With the channel capacity $C_i^{rate}(t)$ and time interval T_i , the data amount Q_i^{data} at the i -th device should ensure that:

$$Q_i^{data} \leq \int_0^{T_i} C_i^{rate}(t) dt \tag{37}$$

To achieve the minimum completion time, the equal sign is selected in (37), and the nearest distance between the UAV and the i -th device is used to calculate $C_i^{rate}(t)$. Consequently, T_i can be determined, and the flying speed V_{zz} is adjusted accordingly, $V_{zz} = d_{O_1O_2}/T_i$. The UAV's propulsion power can be determined based on the curve in Figure 2 corresponding to the flight speed. Numerical results demonstrate that the total minimum completion time is 1432 s, with a total minimum energy consumption of 1826 kJ for task 1. For task 2, the UAV requires a total of 13,191 s to complete the task, consuming a total of 16,819 kJ of energy.

3.3. The Proposed Approach

Finally, the trajectory designs proposed in this study are depicted in Figures 7c and 8c for the two scenarios, respectively. The red dotted lines represent the communication coverage of the UAV, while the small red plus signs indicate the centers of the clustered disks, coinciding with the centers of the circular trajectories. During circular trajectories, the UAV can communicate with multiple IoT devices located within each disk region. The number of disk centers, determined by Algorithm 1, is nine when the maximum coverage radius is 217 m, which is slightly smaller than the limited radius of 220 m. In terms of energy consumption, circular flight proves more efficient than hovering flight when optimal parameters are selected, with V_{cir} set to 8.1 m/s and R_{cir} set to 33.1 m, as reported as the optimal values for a specific UAV with parameters listed in Table 1 [27]. For straight-line flight, the UAV speed is chosen as V_{minE} , as shown in Figure 2. The numerical results demonstrate that the total minimum completion time is 1217 s, with a total minimum energy consumption of 1551 kJ. For task 2, the UAV requires a total of 3048 s to complete the task shown in Figure 8, during which it consumes a total of 3887 kJ of energy.

3.4. Comparison and Discussion

To provide a more comprehensive comparison and evaluate the proposed methodology, additional test cases have been investigated, considering factors such as area size,

data volume, and the number of IoT devices. To clearly present the results, we introduce a new attribute called ‘data density’, which measures the amount of data within a unit area. Subsequently, completion time and energy consumption of the three approaches across various test cases are plotted against the data density of each test case, as illustrated in Figure 10. Table 3 highlights some representative cases, marked with stars in Figure 10.

The proposed approach outperforms the other two classical approaches, regardless of the area size, data volume, and number of IoT devices. It is worth noting that the direct TSP approach is highly energy-inefficient, especially in smaller areas where it fails to harness the potential advantages of multiple communications. While the zigzag approach takes advantage of multiple communications, it neglects the location information of IoT devices, making it less energy-efficient. Additionally, the performance of the zigzag approach degrades in larger areas with sparsely distributed IoT devices, as the task completion distance increases. IoT devices with larger data volumes can further slow down the UAV’s scanning speed. In contrast, the proposed approach not only fully leverages the benefits of multiple communications but also considers the locations of IoT devices. This results in the shortest completion time and lowest energy consumption compared to the other approaches. Finally, compared with the fixed-size disk clustering methods [30,32], the proposed method intelligently clusters IoT devices with optimal coverage radii, enhancing the energy efficiency of both the UAV and the IoT network.

Table 3. Comparison between the different approaches.

IoT Numbers		20 (2 Mb per IoT)			35 (1 Mb per IoT)			50 (0.5 Mb per IoT)		
area [m ²]		500 ²	1000 ²	1500 ²	500 ²	1000 ²	1500 ²	500 ²	1000 ²	1500 ²
TSP	time [s]	4415	4477	4553	7681	7778	7873	2815	2447	3058
	energy [kJ]	4067	4146	4243	7060	7183	7304	2613	2323	2992
Zigzag	time [s]	2591	8951	13,191	1295	4475	8482	648	1423	4241
	energy [kJ]	3303	11,412	16,819	1651	5706	10,812	826	1826	5408
Proposed	time [s]	875	2020	3048	479	1128	2258	441	1217	1398
	energy [kJ]	1116	2576	3887	611	1439	2880	562	1551	1782

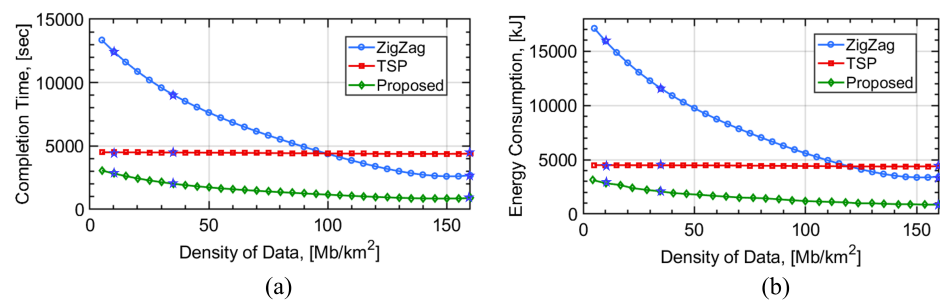


Figure 10. Comparison with respect to energy consumption and completion time. (a) Completion time vs. data density, (b) energy consumption vs. data density. Stars mark the scenarios shown in Table 3.

4. Conclusions

This work presents a novel methodology to optimize UAV trajectory with respect to energy consumption and completion time for a UAV-assisted communication network. By leveraging aerodynamics, a UAV operates more efficiently when flying in a circle rather than hovering. The distribution of IoT devices inevitably affects the deployment of the UAV. Therefore, IoT devices should be intelligently clustered for the UAV to communicate with them. Finally, physically achievable 3D trajectories are essential to ensure the transmission of the UAV from one IoT device cluster to another. Conclusively, the proposed method

reduces the overall communication time and preserves UAV battery energy compared to other benchmark schemes dramatically. The contributions can be summarized as follows:

1. An intelligently designed clustering algorithm is introduced to cluster IoT devices with optimal coverage radii, enhancing the energy efficiency of both the UAV and the IoT network.
2. A methodology for designing trajectories with optimized energy consumption and completion time using circular paths and 3D Dubins curves in UAV-assisted communication networks is derived, providing physically achievable trajectory planning for UAVs.
3. The proposed methodology significantly reduces the overall communication time and conserves more energy compared to other classical benchmark schemes.

Author Contributions: Conceptualization, M.L.; methodology, M.L. and G.J.; software, G.J.; validation, G.J., X.L. and H.Q.; investigation, M.L. and G.J.; writing—original draft preparation, G.J.; writing—review and editing, M.L., X.L. and H.Q. All authors have read and agreed to the published version of the manuscript.

Funding: This research received no external funding.

Data Availability Statement: Source codes are available from the corresponding author M.L. upon request.

Acknowledgments: The authors would like to thank Minjun Qiu and Jia Tan from DJ-Innovations (DJI) for their insightful comments about quadrotor UAVs.

Conflicts of Interest: The authors declare no conflicts of interest.

Abbreviations

The following abbreviations are used in this manuscript:

BLDC	Brushless direct current
CoG	Center of gravity
FCC	Fly–circle–communicate
GA	Genetic Algorithm
IoT	Internet of Things
LoS	Line-of-sight
NLoS	Non-line-of-sight
TSP	Traveling salesman problem
UAV	Unmanned aerial vehicle
WSN	Wireless sensor network

References

1. Boursianis, A.D.; Papadopoulou, M.S.; Diamantoulakis, P.; Liopa-Tsakalidi, A.; Barouchas, P.; Salahas, G.; Karagiannidis, G.; Wan, S.; Goudos, S.K. Internet of things (IoT) and agricultural unmanned aerial vehicles (UAVs) in smart farming: A comprehensive review. *Internet Things* **2022**, *18*, 100187. [[CrossRef](#)]
2. Sony, S.; Laventure, S.; Sadhu, A. A literature review of next-generation smart sensing technology in structural health monitoring. *Struct. Control. Health Monit.* **2019**, *26*, e2321. [[CrossRef](#)]
3. Mozaffari, M.; Saad, W.; Bennis, M.; Nam, Y.H.; Debbah, M. A tutorial on UAVs for wireless networks: Applications, challenges, and open problems. *IEEE Commun. Surv. Tutor.* **2019**, *21*, 2334–2360. [[CrossRef](#)]
4. Zhao, N.; Lu, W.; Sheng, M.; Chen, Y.; Tang, J.; Yu, F.R.; Wong, K.K. UAV-assisted emergency networks in disasters. *IEEE Wirel. Commun.* **2019**, *26*, 45–51. [[CrossRef](#)]
5. Ahmed, S.; Chowdhury, M.Z.; Jang, Y.M. Energy-efficient UAV relaying communications to serve ground nodes. *IEEE Commun. Lett.* **2020**, *24*, 849–852. [[CrossRef](#)]
6. Zhan, C.; Zeng, Y. Aerial–ground cost tradeoff for multi-UAV-enabled data collection in wireless sensor networks. *IEEE Trans. Commun.* **2019**, *68*, 1937–1950. [[CrossRef](#)]
7. Du, R.; Gkatzikis, L.; Fischione, C.; Xiao, M. Energy efficient sensor activation for water distribution networks based on compressive sensing. *IEEE J. Sel. Areas Commun.* **2015**, *33*, 2997–3010. [[CrossRef](#)]

8. Ouyang, F.; Cheng, H.; Lan, Y.; Zhang, Y.; Yin, X.; Hu, J.; Peng, X.; Wang, G.; Chen, S. Automatic delivery and recovery system of Wireless Sensor Networks (WSN) nodes based on UAV for agricultural applications. *Comput. Electron. Agric.* **2019**, *162*, 31–43. [[CrossRef](#)]
9. Baek, H.; Lim, J. Design of future UAV-relay tactical data link for reliable UAV control and situational awareness. *IEEE Commun. Mag.* **2018**, *56*, 144–150. [[CrossRef](#)]
10. Bouabdallah, S.; Noth, A.; Siegwart, R. PID vs LQ control techniques applied to an indoor micro quadrotor. In Proceedings of the 2004 IEEE/RSJ International Conference on Intelligent Robots and Systems (IROS) (IEEE Cat. No. 04CH37566), Sendai, Japan, 28 September–2 October 2004; Volume 3, pp. 2451–2456.
11. Bouabdallah, S.; Siegwart, R. Backstepping and sliding-mode techniques applied to an indoor micro quadrotor. In Proceedings of the 2005 IEEE International Conference on Robotics and Automation, Barcelona, Spain, 18–22 April 2005; pp. 2247–2252.
12. Mahony, R.; Kumar, V.; Corke, P. Multirotor aerial vehicles: Modeling, estimation, and control of quadrotor. *IEEE Robot. Autom. Mag.* **2012**, *19*, 20–32. [[CrossRef](#)]
13. Lee, T.; Leok, M.; McClamroch, N.H. Geometric tracking control of a quadrotor UAV on SE (3). In Proceedings of the 49th IEEE conference on decision and control (CDC), Atlanta, GA, USA, 15–17 December 2010; pp. 5420–5425.
14. Goodarzi, F.; Lee, D.; Lee, T. Geometric nonlinear PID control of a quadrotor UAV on SE (3). In Proceedings of the 2013 European Control Conference (ECC), Zurich, Switzerland, 17–19 July 2013; pp. 3845–3850.
15. Quan, Q.; Fu, R.; Li, M.; Wei, D.; Gao, Y.; Cai, K.Y. Practical distributed control for VTOL UAVs to pass a virtual tube. *IEEE Trans. Intell. Veh.* **2021**, *7*, 342–353. [[CrossRef](#)]
16. Zhu, C.; Chen, J.; Zhang, H. Attitude control for quadrotors under unknown disturbances using triple-step method and nonlinear integral sliding mode. *IEEE Trans. Ind. Electron.* **2022**, *70*, 5004–5012. [[CrossRef](#)]
17. Zeng, Y.; Zhang, R.; Lim, T.J. Wireless communications with unmanned aerial vehicles: Opportunities and challenges. *IEEE Commun. Mag.* **2016**, *54*, 36–42. [[CrossRef](#)]
18. Zhan, C.; Zeng, Y.; Zhang, R. Energy-efficient data collection in UAV enabled wireless sensor network. *IEEE Wirel. Commun. Lett.* **2017**, *7*, 328–331. [[CrossRef](#)]
19. Abeywickrama, H.V.; Jayawickrama, B.A.; He, Y.; Dutkiewicz, E. Empirical power consumption model for uavs. In Proceedings of the 2018 IEEE 88th Vehicular Technology Conference (VTC-Fall), Chicago, IL, USA, 27–30 August 2018; pp. 1–5.
20. Di Franco, C.; Buttazzo, G. Energy-aware coverage path planning of UAVs. In Proceedings of the 2015 IEEE International Conference on Autonomous Robot Systems and Competitions, Vila Real, Portugal, 8–10 April 2015; pp. 111–117.
21. Bramwell, A.R.S.; Balmford, D.; Done, G. *Bramwell's Helicopter Dynamics*; Elsevier: Amsterdam, The Netherlands, 2001.
22. Filippone, A. *Flight Performance of Fixed and Rotary Wing Aircraft*; Elsevier: Amsterdam, The Netherlands, 2006.
23. Zeng, Y.; Xu, J.; Zhang, R. Energy minimization for wireless communication with rotary-wing UAV. *IEEE Trans. Wirel. Commun.* **2019**, *18*, 2329–2345. [[CrossRef](#)]
24. Powers, C.; Mellinger, D.; Kushleyev, A.; Kothmann, B.; Kumar, V. Influence of aerodynamics and proximity effects in quadrotor flight. In *Experimental Robotics: The 13th International Symposium on Experimental Robotics*; Springer: Berlin/Heidelberg, Germany, 2013; pp. 289–302.
25. Fay, G. *Derivation of the Aerodynamic Forces for the Mesicopter Simulation*; Standord University: Stanford, CA, USA, 2001.
26. Hoffmann, G.; Huang, H.; Waslander, S.; Tomlin, C. Quadrotor helicopter flight dynamics and control: Theory and experiment. In Proceedings of the AIAA Guidance, Navigation and Control Conference and Exhibit, Hilton Head, SC, USA, 20–23 August 2007; p. 6461.
27. Jia, G.; Li, C.; Li, M. Energy-Efficient Trajectory Planning for Smart Sensing in IoT Networks Using Quadrotor UAVs. *Sensors* **2022**, *22*, 8729. [[CrossRef](#)] [[PubMed](#)]
28. Yang, D.; Wu, Q.; Zeng, Y.; Zhang, R. Energy tradeoff in ground-to-UAV communication via trajectory design. *IEEE Trans. Veh. Technol.* **2018**, *67*, 6721–6726. [[CrossRef](#)]
29. Ning, Z.; Yang, Y.; Wang, X.; Guo, L.; Gao, X.; Guo, S.; Wang, G. Dynamic computation offloading and server deployment for UAV-enabled multi-access edge computing. *IEEE Trans. Mob. Comput.* **2021**, *22*, 2628–2644. [[CrossRef](#)]
30. Zeng, Y.; Xu, X.; Zhang, R. Trajectory design for completion time minimization in UAV-enabled multicasting. *IEEE Trans. Wirel. Commun.* **2018**, *17*, 2233–2246. [[CrossRef](#)]
31. Tran, D.H.; Vu, T.X.; Chatzinotas, S.; ShahbazPanahi, S.; Ottersten, B. Coarse trajectory design for energy minimization in UAV-enabled. *IEEE Trans. Veh. Technol.* **2020**, *69*, 9483–9496. [[CrossRef](#)]
32. Lyu, J.; Zeng, Y.; Zhang, R.; Lim, T.J. Placement optimization of UAV-mounted mobile base stations. *IEEE Commun. Lett.* **2016**, *21*, 604–607. [[CrossRef](#)]
33. Galkin, B.; Kibilda, J.; DaSilva, L.A. Deployment of UAV-mounted access points according to spatial user locations in two-tier cellular networks. In Proceedings of the 2016 Wireless Days (WD), Toulouse, France, 23–25 March 2016; pp. 1–6.
34. Li, F.; He, C.; Li, X.; Peng, J.; Yang, K. Geometric Analysis-Based 3D Anti-Block UAV Deployment for mmWave Communications. *IEEE Commun. Lett.* **2022**, *26*, 2799–2803. [[CrossRef](#)]
35. Qu, H.; Zhang, W.; Zhao, J.; Luan, Z.; Chang, C. Rapid deployment of UAVs based on bandwidth resources in emergency scenarios. In Proceedings of the 2020 Information Communication Technologies Conference (ICTC), Nanjing, China, 29–31 May 2020; pp. 86–90.

36. Mozaffari, M.; Saad, W.; Bennis, M.; Debbah, M. Unmanned aerial vehicle with underlaid device-to-device communications: Performance and tradeoffs. *IEEE Trans. Wirel. Commun.* **2016**, *15*, 3949–3963. [[CrossRef](#)]
37. Mozaffari, M.; Saad, W.; Bennis, M.; Debbah, M. Efficient deployment of multiple unmanned aerial vehicles for optimal wireless coverage. *IEEE Commun. Lett.* **2016**, *20*, 1647–1650. [[CrossRef](#)]
38. Al-Hourani, A.; Kandeepan, S.; Lardner, S. Optimal LAP altitude for maximum coverage. *IEEE Wirel. Commun. Lett.* **2014**, *3*, 569–572. [[CrossRef](#)]
39. Jia, G.; Ding, B.; Li, M. Mathematical Derivation and Simulation Verification for Aggressive Quadrotor Perching Control. In Proceedings of the 2021 China Automation Congress (CAC), Beijing, China, 22–24 October 2021; pp. 5319–5324.
40. Zhu, B.; Bedeer, E.; Nguyen, H.H.; Barton, R.; Henry, J. UAV trajectory planning in wireless sensor networks for energy consumption minimization by deep reinforcement learning. *IEEE Trans. Veh. Technol.* **2021**, *70*, 9540–9554. [[CrossRef](#)]
41. Stuart, S. *DC Motors, Speed Controls, Servo Systems: An Engineering Handbook*; Elsevier: Amsterdam, The Netherlands, 2013.
42. Bor-Yaliniz, R.I.; El-Keyi, A.; Yanikomeroglu, H. Efficient 3-D placement of an aerial base station in next generation cellular networks. In Proceedings of the 2016 IEEE International Conference on Communications (ICC), Kuala Lumpur, Malaysia, 22–27 May 2016; pp. 1–5.
43. Laporte, G. The traveling salesman problem: An overview of exact and approximate algorithms. *Eur. J. Oper. Res.* **1992**, *59*, 231–247. [[CrossRef](#)]
44. Potvin, J.Y. Genetic algorithms for the traveling salesman problem. *Ann. Oper. Res.* **1996**, *63*, 337–370. [[CrossRef](#)]
45. Aarts, E.H.; Korst, J.H.; van Laarhoven, P.J. A quantitative analysis of the simulated annealing algorithm: A case study for the traveling salesman problem. *J. Stat. Phys.* **1988**, *50*, 187–206. [[CrossRef](#)]
46. Shkel, A.M.; Lumelsky, V. Classification of the Dubins set. *Robot. Auton. Syst.* **2001**, *34*, 179–202. [[CrossRef](#)]
47. Song, Q.; Jin, S.; Zheng, F.C. Completion time and energy consumption minimization for UAV-enabled multicasting. *IEEE Wirel. Commun. Lett.* **2019**, *8*, 821–824. [[CrossRef](#)]

Disclaimer/Publisher’s Note: The statements, opinions and data contained in all publications are solely those of the individual author(s) and contributor(s) and not of MDPI and/or the editor(s). MDPI and/or the editor(s) disclaim responsibility for any injury to people or property resulting from any ideas, methods, instructions or products referred to in the content.